

# Gravitational time dilation in quantum clock interferometry with entangled multi-photon states and quantum memories

Mustafa Gündoğan,<sup>1,\*</sup> Roy Barzel,<sup>2</sup> and Dennis Rätzel<sup>2,3,†</sup>

<sup>1</sup>*Institut für Physik and Center for the Science of Materials Berlin (CSMB), Humboldt-Universität zu Berlin, Berlin, 12489, Germany*

<sup>2</sup>*ZARM, Universität Bremen, Am Fallturm 2, 28359 Bremen, Germany*

<sup>3</sup>*Vienna Center for Quantum Science and Technology, Atominstitut, TU Wien, Stadionallee 2, 1020 Vienna, Austria*

Gravitational time dilation implies that clocks held at different heights accumulate different proper times. We analyze a memory-assisted quantum clock interferometer in which a frequency-bin photonic clock is stored in two vertically separated quantum memories for a controllable duration, such that the joint state evolves in a quantum superposition of two proper times. After retrieval, the photonic modes interfere in a Hong–Ou–Mandel (HOM) interferometer, for which we derive analytic expressions for the resulting multiphoton detection statistics. Extending this HOM-based scheme from entangled photon pairs to frequency-entangled  $2N$ -photon inputs, we show that the proper-time dependent phase is amplified by a factor  $N$ , leading to an  $N$ -times faster collapse and revival of the interference signal compared with the two-photon case. Incorporating finite memory efficiency and lifetime, we identify regimes where this modulation remains observable. For parameters compatible with demonstrated Rb and Cs memories and achievable optical frequency separations, the first collapse occurs for height differences in the order of 10–100 m with subsecond to few-second storage times, while suitable rare-earth ion and alkali memory combinations can reduce the required height to the few-metre scale. These results establish near-term laboratory conditions for observing entanglement dynamics driven by gravitational time dilation in a photonic platform.

Tests of gravity in the quantum regime require systems in which general relativistic effects influence genuinely quantum degrees of freedom. Beyond Newtonian and post-Newtonian gravitational phase shifts such as the Colella–Overhauser–Werner effect [1], a qualitatively different phenomenon occurs when a quantum system possesses an internal two-level structure that functions as a clock. If the spatial wavefunction is coherently split between regions of different gravitational potential, the internal state evolves with the respective local proper times. This produces a coupling between internal and external degrees of freedom that generates entanglement and leads to a reduction and revival of interferometric visibility. The effect was identified by Zych *et al.* [2] as a direct operational signature of proper time in quantum mechanics. It differs from gravitationally induced phase shifts that modify only the interferometer phase [3], such as the gravitational Aharonov–Bohm signal observed in atom interferometry [4], where no visibility loss occurs because no path-dependent clock information is encoded. Related time-dilation–induced decoherence mechanisms in composite systems were discussed before [5], though these do not rely on interferometric which-path information.

Several systems have been proposed for observing general relativistic proper-time effects in a quantum setting, including matter-wave interferometers [6–8], trapped electrons [9], single photons [10], and entangled clock architectures [11–14]. For photons, however, free-space

propagation would require interferometers with vertical separations of tens of kilometers, which renders experiments impractical [10, 15]. A viable pathway was introduced in previous work by employing quantum memories to map photonic excitations to long-lived atomic states, allowing the proper-time difference to accumulate while the excitation remains localized [16]. This approach reduces the required spatial scale by many orders of magnitude. Other relativistic photonic effects, for example gravitationally induced polarization rotation [17], do not require interferometric geometries and probe different physical mechanisms, whereas visibility modulation from proper-time entanglement specifically necessitates either extreme arm separations or a mechanism that boosts proper-time accumulation, such as quantum memories.

Building on these foundations, in this work, we generalize gravitational clock interferometry to genuine  $2N$ -photon entangled states which would yield enhanced sensitivity, multiplying effective phase differences and therefore enabling the detection of gravitational time dilation effects at reduced scales. By integrating path–frequency entangled multi-photon states [18] based on frequency bins [16, 19–23], with quantum memories, this work further compactifies the required interferometers to around a few meter scale with realistic experimental parameters.

The protocol would start with the preparation of a multi-photon entangled state of the form

$$|\psi_{\text{HOM}}\rangle = N_{\text{HOM}} \left[ \hat{a}_{U1}^{\dagger N} \hat{a}_{L2}^{\dagger N} + e^{i\varphi} \hat{a}_{U2}^{\dagger N} \hat{a}_{L1}^{\dagger N} \right] |0\rangle \quad (1)$$

where  $\hat{a}_{\sigma i}^{\dagger}$  is the photonic creation operator with  $i \in \{1, 2\}$  denoting separate frequency bins,  $\Omega_i$ ,  $\sigma = \{U, L\}$

\* [mustafa.guendogan@physik.hu-berlin.de](mailto:mustafa.guendogan@physik.hu-berlin.de)

† [dennis.raetzel@zarm.uni-bremen.de](mailto:dennis.raetzel@zarm.uni-bremen.de)

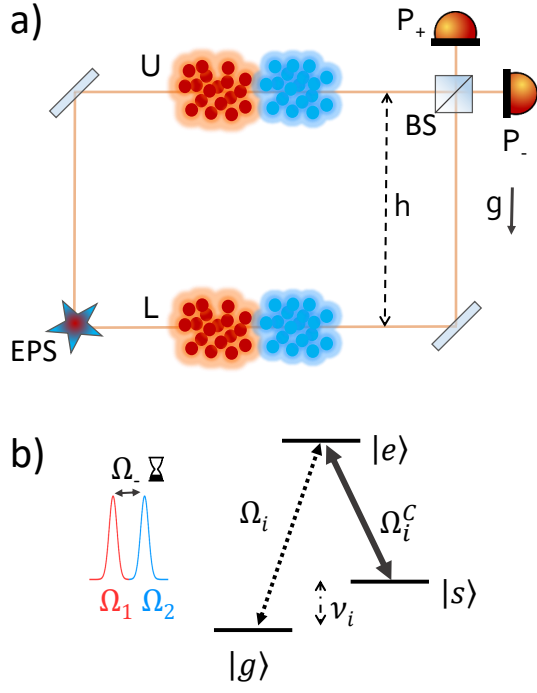


FIG. 1. Experimental proposal: a) The vertical interferometer with two quantum memories in each arm for frequency components  $\Omega_{1,2}$ . The entangled pair source (EPS) generates the state in Eq.1 and each frequency component is stored in corresponding quantum memories in upper (U) and lower (L) branches. After local storage time  $t_s$ , the memories are read out and the resultant state is sent to the BS for the eventual parity detection. b) *Quantum clock* with photons and the relevant  $\Lambda$ -scheme for the memories.: a  $2N$ -photon state (Eq.1) from  $\Omega_{1,2}$  frequency components which are resonant with memories with corresponding colours.  $\Omega_i$  denotes the input frequency;  $\Omega_i^C$  is the corresponding control pulse frequency for storage and retrieval and  $\nu_i$  is the spin-wave frequency.

denotes upper and lower arms of the interferometer,  $N_{\text{HOM}} = (\sqrt{2}N!)^{-1}$  is the normalization factor (see Appendix A for detailed derivation) and  $\varphi$  is a fixed phase defined by the photon source. This state represents a coherent superposition in which either  $N$  photons at frequency  $\Omega_1$  propagate in the upper arm and  $N$  photons at frequency  $\Omega_2$  in the lower arm, or vice versa. We also assume that the separation between these frequency bins are much larger than the bandwidth of individual photons. We note that, as already shown in the appendix of [16], the chosen symmetries of the probe state is crucial for the protocol. In particular, superpositions of states with identical frequencies of all photons (frequency-aligned states) are not affected, similar to the case of superpositions of states where all photons occupying only one arm of the interferometer [24].

The vertical interferometer has a height of  $h$  with quantum memories in each arm that are capable of storing in-

dividual  $\Omega_i$  frequency components (Fig.1a). This height difference results in first-order gravitational redshift factor of  $\Theta_\sigma \approx 1 + gh_\sigma/c^2$ , where  $g$  is the gravitational acceleration at altitude  $h_\sigma$ . This approximation is valid for small height differences when curvature and the difference in the special relativistic time dilation can be neglected. We work with this approximation since we focus on terrestrial experiments with  $h = 10^1 - 10^2$  m of height differences.

After the generation of the state  $|\psi_{\text{HOM}}\rangle$ , each spatial branch now propagates to a different height in the gravitational potential, leading to a shift of the frequencies to  $\tilde{\Omega}_{\sigma,i} = \Omega_i/\Theta_\sigma$  (adding a tilde to denote local quantities), and enters a long-lived [25],  $\Lambda$ -type QM for a local laboratory time  $\tau_{\sigma s}$ . A write pulse, which can be modeled as a  $\pi/2$ -mode swap [26] (see [16] for details), converts photons at frequencies  $\tilde{\Omega}_{\sigma,i}$  into collective spin waves with frequencies  $\tilde{\nu}_{\sigma,i}$  after proper storage time  $\tau_{\sigma s} = t_s/\Theta_\sigma$  an identical read pulse retrieves these excitations and converts them back to optical photons. For each individual photon, the evolution is

$$\begin{aligned} \hat{a}_{\sigma,i}^\dagger &\xrightarrow{\text{write}} e^{i\phi_{\sigma i}^w} \hat{S}_{\sigma i}^\dagger \xrightarrow{\text{storage}} e^{i(\phi_{\sigma i}^w + \tilde{\nu}_{\sigma i} \tau_{\sigma s})} \hat{S}_{\sigma i}^\dagger \\ &\xrightarrow{\text{read}} e^{i(\phi_{\sigma i}^w - \phi_{\sigma i}^r + \tilde{\nu}_{\sigma i} \tau_{\sigma s})} \hat{a}_{\sigma,i}^\dagger. \end{aligned} \quad (2)$$

where  $\phi_{\sigma i}^w$  and  $\phi_{\sigma i}^r$  denote the write-in and read-out pulse phases. The negative sign is due to the time-reversal character of the read-out process with respect to write-in [26]. Assuming that the control laser is phase-coherent during the storage period,  $\phi_{\sigma i}^r = \phi_{\sigma i}^w + \tau_{\sigma s} \tilde{\Omega}_{\sigma i}^{(w/r)}$ , where the frequencies are constrained to  $\tilde{\Omega}_{\sigma i} = \tilde{\nu}_{\sigma i} + \tilde{\Omega}_{\sigma i}^{(w/r)}$ . For an  $N$  photon wavepacket the exponent is multiplied by  $N$ .

The state at the output of the memories becomes

$$|\psi_{\text{HOM}}\rangle_{\text{mem}} = N_{\text{HOM}} \left[ \hat{a}_{U1}^{\dagger N} \hat{a}_{L2}^{\dagger N} + e^{i\phi_{\text{HOM}}} \hat{a}_{U2}^{\dagger N} \hat{a}_{L1}^{\dagger N}, \right] |0\rangle \quad (3)$$

with  $\phi_{\text{HOM}} = N[\Omega_- (\tau_{Us}/\Theta_U - \tau_{Ls}/\Theta_L)] + \varphi$  and  $\Omega_- = \Omega_2 - \Omega_1$ . With equal storage times, i.e.,  $\tau_{Us} = \tau_{Ls} = \tau_s$ , in both arms, this simplifies to [16]

$$\phi_{\text{HOM}} = N(\Omega_- \Delta_{\Theta-1} \tau_s) + \varphi. \quad (4)$$

where  $\Delta_{\Theta-1} = 1/\Theta_U - 1/\Theta_L$  is the differential inverse redshift between the two arms. The photonic state in Equation 3 is then mixed into constructive ( $\oplus$ ) and destructive ( $\ominus$ ) ports by the beam splitter via the transformations  $\hat{a}_{U,i}^\dagger \rightarrow \frac{1}{\sqrt{2}}(\hat{a}_{\oplus,i}^\dagger - \hat{a}_{\ominus,i}^\dagger)$  and  $\hat{a}_{L,i}^\dagger \rightarrow \frac{1}{\sqrt{2}}(\hat{a}_{\oplus,i}^\dagger + \hat{a}_{\ominus,i}^\dagger)$ ,

$$\begin{aligned} |\Psi_{\text{BS}}\rangle &= \frac{N_{\text{HOM}}}{2^N} \left[ \left( \hat{a}_{\oplus 1}^\dagger - \hat{a}_{\ominus 1}^\dagger \right)^N \left( \hat{a}_{\oplus 2}^\dagger + \hat{a}_{\ominus 2}^\dagger \right)^N \right. \\ &\quad \left. + e^{i\phi_{\text{HOM}}} \left( \hat{a}_{\oplus 2}^\dagger - \hat{a}_{\ominus 2}^\dagger \right)^N \left( \hat{a}_{\oplus 1}^\dagger + \hat{a}_{\ominus 1}^\dagger \right)^N \right] |0\rangle. \end{aligned} \quad (5)$$

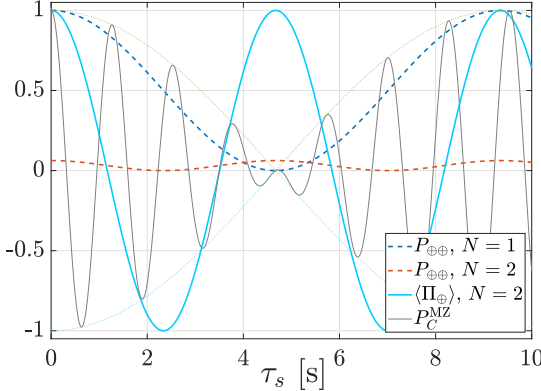


FIG. 2. Plot of Eqs. (8) and (12) for Rubidium (780 nm) and Cesium (894 nm) quantum memories, corresponding to  $\Omega_- = 2\pi \times 49$  THz and a vertical separation of  $h = 20$  m, as a function of the memory time  $\tau_s$ . The expected signal from a Mach-Zehnder interferometer using a single-photon frequency bin (i.e. N00N with  $N=1$ ) [16] is also shown for comparison, where the fast oscillations with  $\Omega_+ = \Omega_2 + \Omega_1$  are also visible. The initial global phase,  $\phi$ , is set to 0.

The act of the beam splitter is effectively to distribute each  $N$ -photon component across two ports binomially with the proper phase relation among them. Expansion of Eq. 5 would yield the following explicit form,

$$|\Psi_{\text{BS}}\rangle = \frac{N_{\text{HOM}}}{2^N} \sum_{k,l=0}^N \binom{N}{k} \binom{N}{l} \left[ (-1)^k + e^{i\phi_{\text{HOM}}} (-1)^l \right] \times (\hat{a}_{\oplus 1}^\dagger)^{N-k} (\hat{a}_{\ominus 1}^\dagger)^k (\hat{a}_{\oplus 2}^\dagger)^{N-l} (\hat{a}_{\ominus 2}^\dagger)^l |0\rangle, \quad (6)$$

where  $k$  denotes the number of photons at frequency  $\Omega_1$  exiting through port  $\ominus$ , and  $l$  denotes the number of  $\Omega_2$  photons exiting through the same port. As a starting point, we are interested in the case where all  $2N$  photons leave from the same port. In order to find the probability of all the photons leaving through, say, port  $\oplus$ , we set  $k = l = 0$  in Eq. 6 to find the resultant conditional state:

$$|\Psi_{\text{BS}}\rangle_{\oplus\oplus} = N_{\text{HOM}} \frac{1 + e^{i\phi_{\text{HOM}}}}{2^N} (\hat{a}_{\oplus 1}^\dagger)^N (\hat{a}_{\oplus 2}^\dagger)^N |0\rangle, \quad (7)$$

whose associated probability will be given by

$$P_{\oplus\oplus} = |\langle N, N | \Psi_{\text{BS}} \rangle_{\oplus\oplus}|^2 = \left( \frac{N_{\text{HOM}}}{2^{N-1}} \right)^2 (1 + \cos(\phi_{\text{HOM}})). \quad (8)$$

which is consistent with Ref. [16] for  $N = 1$ . Measuring this probability requires photon-number-resolving (PNR) detection. This can be achieved either with true

PNR detectors or, more crudely, by splitting each output into  $2N$  spatial modes and placing a non-number resolving, i.e. bucket, detector on each. Although the latter approach is far less efficient, it provides a practical workaround when PNR detectors are not available. However, since we have to condition on the detection of all  $2N$  photons to leave from a specific port, this approach is still not efficient, as can be seen from the prefactor  $(N_{\text{HOM}}/2^{N-1})^2$ .

As an alternative, instead of the subset of cases considered above, one could measure the parity of the photon number at the output ports. We define the parity operator [27, 28] on a given output port, say,  $\oplus$ , as

$$\hat{\Pi}_{\oplus} := (-1)^{\hat{n}_{\oplus 1} + \hat{n}_{\oplus 2}} = e^{i\pi(\hat{n}_{\oplus 1} + \hat{n}_{\oplus 2})}. \quad (9)$$

Since the total photon number is fixed to  $2N$  (even), the two parities are identical ( $\hat{\Pi}_{\oplus} = \hat{\Pi}_{\ominus}$ ) and their product is the identity,  $\hat{\Pi}_{\oplus} \hat{\Pi}_{\ominus} = (-1)^{\hat{n}_{\oplus 1} + \hat{n}_{\oplus 2} + \hat{n}_{\ominus 1} + \hat{n}_{\ominus 2}} = (-1)^{2N} = \mathbb{1}$ . The expectation value of the parity operator then directly measures the even-odd photon-number imbalance at one output port:

$$\langle \hat{\Pi}_{\oplus} \rangle = \sum_{k,l} (-1)^{k+l} P_{k,l} = P_{\oplus e} - P_{\oplus o} \quad (10)$$

where  $P_{\oplus e}$  and  $P_{\oplus o}$  are the sums of all  $P_{k,l}$  with  $k+l$  even and odd, respectively, and the individual probabilities follow directly from Eq. (6) (see Appendix B)

$$P_{k,l} = \frac{\binom{N}{k} \binom{N}{l}}{2^{2N}} \left[ 1 + (-1)^{k+l} \cos(\phi_{\text{HOM}}) \right]. \quad (11)$$

By summing the individual probabilities, we find (see Appendix B)  $P_{\oplus e} = (1 + \cos(\phi_{\text{HOM}}))/2$  and  $P_{\oplus o} = (1 - \cos(\phi_{\text{HOM}}))/2$ . With this, the expectation value of the parity operator of port  $\oplus$  becomes

$$\langle \hat{\Pi}_{\oplus} \rangle = P_{\oplus e} - P_{\oplus o} = \cos(\phi_{\text{HOM}}). \quad (12)$$

This shows that the cosine dependence originates from interference between the two indistinguishable multiphoton paths, with  $\phi_{\text{HOM}}$  given in Eq.(4). Thus the even-odd population imbalance follows the interference phase with an  $N$ -fold enhancement inside  $\phi_{\text{HOM}}$  [29], without the  $(N_{\text{HOM}}/2^{N-1})^2$  penalty of the all photons in one port events (Eq. 8). In the absence of gravitational time dilation the phase in Eq. (12) becomes time independent. For equal local storage times one would have  $\Delta\Theta^{-1} = 0$ , so that  $\varphi_{\text{HOM}} = \phi$  and the parity signal reduces to a constant,  $\langle \hat{\Pi}_{\oplus} \rangle = \cos(\phi)$ , independent of  $\tau_s$ . Thus, in a scenario where no proper-time difference is accumulated, the expected behaviour is a flat interferogram. Any statistically significant deviation from this constant baseline constitutes direct evidence that the two arms have acquired a relative proper-time difference, and therefore serves as an operational witness of proper-time entanglement generated by the gravitational redshift. This dynamics can be detected via PNR detectors. With this,

the required memory time to reach the first zero [2, 16] of the HOM interferogram becomes

$$\tau_{\text{ent}}^{(N)} = \frac{\pi}{2N \Delta\Theta^{-1} \Omega_-}, \quad (13)$$

The key observation is that the interference contrast now vanishes  $N$  times faster than in the ordinary two-photon case. Operationally, the relevant resource is the product  $h \tau_{\text{ent}}$ , which is reduced by a factor  $1/N$ : for fixed  $\tau_{\text{ent}}$  one needs  $h \rightarrow h/N$ , and likewise, for fixed  $h$  one needs  $\tau_{\text{ent}} \rightarrow \tau_{\text{ent}}/N$ , or the reduction can be shared (e.g.,  $h \rightarrow h/\sqrt{N}$  and  $\tau_{\text{ent}} \rightarrow \tau_{\text{ent}}/\sqrt{N}$ ).

By contrast, no such enhancement can be observed if one injects an  $N$ -photon frequency-N00N state of the form [30]

$$|\Psi_{\text{MZ}}\rangle = \frac{1}{\sqrt{2}} \left( |N, 0\rangle_{\Omega_1, \Omega_2; A} + e^{i\phi} |0, N\rangle_{\Omega_1, \Omega_2; A} \right) \quad (14)$$

into a Mach–Zehnder (MZ) interferometer through port A. The usual  $N$ -photon enhancement requires that the phase be written on a distinguishable path degree of freedom [31, 32], as in Eq. 3, whereas the N00N superposition in this case resides in frequency domain. The first 50:50 beam splitter therefore distributes each  $N$ -photon bundle binomially between the two arms, randomising the path information and eliminating the  $N$ -fold phase sensitivity. As a result, the interferometer reverts to the standard scaling. Another main difference between the two scenarios is that the MZ is sensitive to fast oscillations with  $\Omega_+ = \Omega_1 + \Omega_2$  [16]

$$P_C^{\text{MZ}} = \cos(\Omega_- \Delta\Theta^{-1} \tau_s/2) \cos(\Omega_+ \Delta\Theta^{-1} \tau_s/2), \quad (15)$$

while these do not appear in the HOM interferogram which only oscillates with  $\Omega_-$ . Figure 2 summarizes the qualitative differences between HOM-based clock interferometry and a Mach–Zehnder (MZ) readout for the same optical frequencies and height difference. For the HOM protocol, both the post-selected bunching probability  $P_{\oplus\oplus}$  [Eq. (8)] and the parity observable  $\langle \hat{\Pi}_{\oplus} \rangle$  [Eq. (12)] depend only on the *difference* frequency  $\Omega_- = \Omega_2 - \Omega_1$  through the phase  $\varphi_{\text{HOM}} = N \Omega_- \Delta\Theta^{-1} \tau_s + \phi$ , leading to an 2-fold faster oscillation when going from  $N = 1$  to  $N = 2$ . In contrast, the MZ coherence signal contains the additional factor  $\cos(\Omega_+ \Delta\Theta^{-1} \tau_s/2)$  [Eq. (15)], so that fast oscillations associated with  $\Omega_+ = \Omega_1 + \Omega_2$  appear on top of the slower envelope set by  $\Omega_-$ . Finally, Fig. 2 highlights why parity measurements are preferable for larger photon numbers: although  $P_{\oplus\oplus}$  exhibits the same phase dependence, its magnitude rapidly decreases with  $N$  due to the required post-selection on events where all  $2N$  photons exit the same output port, whereas  $\langle \hat{\Pi}_{\oplus} \rangle$  accesses the phase using the full photon-number distribution at the outputs. Figure 3, in turn, presents a log–log color map  $\tau_{\text{ent}}$  (13) as a function of height  $h$  and the optical frequency difference  $\Delta f = \Omega_-/(2\pi)$ . The markers indicate experimentally relevant operating points: (i) a narrow spectral bin

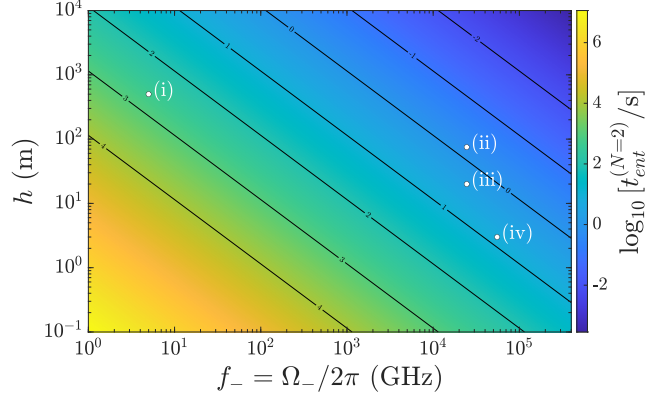


FIG. 3. Log–log map of the gravitationally induced entanglement collapse time  $t_{\text{ent}}$  as a function of the differential optical frequency  $\Delta f = \Omega_-/(2\pi)$  and height  $h$  for  $N = 2$ . The contour lines indicate equal collapse times from  $10^{-2}$  s to  $10^4$  s. Different specific configurations are marked. (i)  $\Delta f = 10$  GHz at 500 m, which could be realized by using different spectral regions within the same rare-earth doped memory; (ii) and (iii) Rb – Cs memory pairs at 75 m and 20 m; (iv)  $\text{Pr}^{3+} : \text{Y}_2\text{SiO}_5$  – Rb pair at 3 m.

$\Delta f = 10$  GHz stored at different frequency bins within the inhomogeneous broadening of a single rare-earth-doped memory [33, 34]; (ii)–(iii) Rb [25, 26, 35, 36]–Cs [37–39] memory pairs at  $h = 75$  m and  $h = 20$  m; and (iv) a  $\text{Pr}^{3+} : \text{Y}_2\text{SiO}_5$  [33]–Rb combination around  $h = 3$  m.

We model memory loss as a fictitious beam splitter of transmissivity  $\eta_m$  that couples the signal mode  $\hat{a}^\dagger$  to an environmental vacuum mode  $\hat{v}^\dagger$  via  $\hat{a}^\dagger \rightarrow \sqrt{\eta_m} \hat{a}^\dagger + \sqrt{1 - \eta_m} \hat{v}^\dagger$ . For an  $N$ -photon excitation in interferometer arm  $\sigma$  this implies  $(\hat{a}_\sigma^\dagger)^N \rightarrow \sum_{k_\sigma=0}^N \binom{N}{k_\sigma} (\sqrt{\eta_m} \hat{a}_\sigma^\dagger)^{N-k_\sigma} (\sqrt{1 - \eta_m} \hat{v}_\sigma^\dagger)^{k_\sigma}$ . The terms with  $k_\sigma > 0$  correspond to events in which at least one photon is lost, thus leaving fewer than  $2N$  photons. Since our parity signal is defined on the  $2N$ -photon subspace, we project onto the no-loss component  $k_\sigma = 0$ , which acquires an amplitude factor  $(\sqrt{\eta_m})^N$  per arm. For both arms combined, the  $2N$ -photon component therefore survives with probability  $\eta_m^{2N}$  per heralded input, so the parity signal described by Eq. (12) is detected with a reduced  $2N$ -photon count rate proportional to  $\eta_m^{2N}$ .

Finally, we comment on the relation to photonic clock interferometry based on the photon arrival time [10]. The photonic adaptation in Ref. [10] encodes the clock in the photons paths: a single broad spectral peak (short pulse) accumulates a relative arrival-time offset  $\Delta\tau$  (Shapiro delay) between paths at different heights. For a Gaussian wavepacket, the HOM interferogram decays as a function of the relative time delay between the two arms, with no intrinsic revivals. Observing a sizable effect, therefore, requires ultrashort (fs to sub-fs) pulses such that  $\Delta\tau \gtrsim \tau_{\text{coh}}$  with  $\Delta\tau \simeq lgh/c^3$  [10]. This would require extremely large interferometer areas ( $\gtrsim 10^3$  km $^2$  for

pulse durations of order 1 fs), which in turn pose serious challenges in terms of loss, dispersion management, and phase stability.

In our approach, the temporal envelopes can be long since the clock is encoded in two narrow frequency bins that form an effective two-level system. The corresponding excitations are stored in quantum memories at different heights for equal local storage times  $\tau_s^U = \tau_s^L = \tau_s$ . Gravity imprints a proper-time dependent phase between the frequency components, which leads to collapse and revival of bunching and anti-bunching probabilities governed by this internal phase rather than by an arrival-time walk-off. The main result is that now the required photonic interferometer area is reduced to  $\mathcal{O}(10^{-4} \text{ km}^2)$ , which is readily available [40–42]. Required memory times are within experimental reach too, while generation of the input state  $|\psi_{\text{HOM}}\rangle$  in Eq. 1 would require complicated operations, such as frequency beam splitters and heralding with PNR detectors. However, initial steps towards generating such states have already been taken in the form of frequency-bin [23] entanglement [21, 43] and N00N states [30]. Furthermore, heralded generation of complex multiphoton states is also an active research field and significant advance has been made in the recent years [44].

In conclusion, we have extended the memory-assisted quantum clock-interferometry framework introduced in Ref. [16] to multi-photon frequency-bin entangled inputs, and shown that genuinely general-relativistic time-dilation effects on quantum superpositions can, in principle, be observed on photonic platforms with experimentally accessible parameters. In contrast to earlier photonic proposals [10, 15], our approach leverages quantum memories, enabling a pathway toward observing such effects in realistic interferometers with meter-scale baselines. Furthermore, our scheme provides a concrete instance of quantum metrological advantage in a relativistic setting: the  $N$ -fold enhancement of the proper-time-dependent clock phase directly translates into reduced requirements on interferometer height, area, and storage time for a given target signal. Our framework can also be extended to scenarios with more than two spacetime branches [14] or combined with vertical scanning of the interferometer height [15], offering potential routes to extract information about spacetime curvature. This work thus marks a step forward in employing quantum optical tools to probe the interface between gravity and quantum physics.

*Acknowledgments.* The authors thank M. Krutzik for fruitful discussions and comments on this manuscript. M.G. acknowledges the support from the DLR through funds provided by the Federal Ministry for Economic Affairs and Climate Action (Bundesministerium für Wirtschaft und Klimaschutz, BMWK) under Grant No. 50WM2347 and Einstein Foundation Berlin for support. D.R. acknowledges support by the Federal Ministry of Education and Research of Germany in the project Open6GHub (grant number: 16KISK016) and

the Deutsche Forschungsgemeinschaft (DFG, German Research Foundation) under Germanys Excellence Strategy – EXC-2123 QuantumFrontiers – 390837967.

## Appendix A: Derivation of the normalization $N_{\text{HOM}}$

We start with the pre-beam-splitter state (1)

$$|\Psi_{\text{in}}\rangle = N_{\text{HOM}} \left[ a_{U1}^{\dagger N} a_{L2}^{\dagger N} + e^{i\phi} a_{U2}^{\dagger N} a_{L1}^{\dagger N} \right] |0\rangle, \quad (\text{A1})$$

and define the two branches

$$\begin{aligned} |\psi_1\rangle &:= (a_{U1}^{\dagger})^N (a_{L2}^{\dagger})^N |0\rangle, \\ |\psi_2\rangle &:= (a_{U2}^{\dagger})^N (a_{L1}^{\dagger})^N |0\rangle. \end{aligned} \quad (\text{A2})$$

The norm of (A1) is

$$\begin{aligned} \langle \Psi_{\text{in}} | \Psi_{\text{in}} \rangle &= |N_{\text{HOM}}|^2 \left( \langle \psi_1 | \psi_1 \rangle + \langle \psi_2 | \psi_2 \rangle \right. \\ &\quad \left. + e^{i\phi} \langle \psi_1 | \psi_2 \rangle + e^{-i\phi} \langle \psi_2 | \psi_1 \rangle \right). \end{aligned} \quad (\text{A3})$$

Using commutation between different modes, one finds

$$\begin{aligned} \langle \psi_1 | \psi_2 \rangle &= \langle 0 | a_{L2}^N a_{U1}^N a_{U2}^{\dagger N} a_{L1}^{\dagger N} | 0 \rangle \\ &= \langle 0 | a_{L2}^N a_{U2}^{\dagger N} a_{L1}^{\dagger N} a_{U1}^N | 0 \rangle = 0. \end{aligned} \quad (\text{A4})$$

and similarly  $\langle \psi_2 | \psi_1 \rangle = 0$ . Thus only the diagonal terms contribute. For a single bosonic mode  $a$  one has  $(a^{\dagger})^N |0\rangle = \sqrt{N!} |N\rangle$  and  $\langle 0 | a^N = \sqrt{N!} \langle N |$ , hence  $\langle 0 | a^N a^{\dagger N} | 0 \rangle = N!$ . Using independence of modes one finds,

$$\begin{aligned} \langle \psi_1 | \psi_1 \rangle &= \langle 0 | a_{U1}^N a_{U1}^{\dagger N} | 0 \rangle \langle 0 | a_{L2}^N a_{L2}^{\dagger N} | 0 \rangle \\ &= N! N!, \end{aligned} \quad (\text{A5})$$

and by symmetry  $\langle \psi_2 | \psi_2 \rangle = N! N!$ . For the final step, we substitute (A4) and (A5) into (A3)

$$\langle \Psi_{\text{in}} | \Psi_{\text{in}} \rangle = 2 |N_{\text{HOM}}|^2 N! N!. \quad (\text{A6})$$

Imposing  $\langle \Psi_{\text{in}} | \Psi_{\text{in}} \rangle = 1$  yields

$$N_{\text{HOM}} = \frac{1}{\sqrt{2 N! N!}}. \quad (\text{A7})$$

## Appendix B: Derivation of Eq. (12)

Taking into account that

$$\begin{aligned} \hat{\Pi}_{\ominus} (\hat{a}_{\oplus 1}^{\dagger})^{N-k} (\hat{a}_{\ominus 1}^{\dagger})^k (\hat{a}_{\oplus 2}^{\dagger})^{N-l} (\hat{a}_{\ominus 2}^{\dagger})^l |0\rangle \\ = e^{i\pi(2N-k-l)} (\hat{a}_{\oplus 1}^{\dagger})^{N-k} (\hat{a}_{\ominus 1}^{\dagger})^k (\hat{a}_{\oplus 2}^{\dagger})^{N-l} (\hat{a}_{\ominus 2}^{\dagger})^l |0\rangle \end{aligned} \quad (\text{B1})$$

and  $e^{i\pi(2N-k-l)} = e^{i\pi(k+l)}$  for integers  $k, l$ , we obtain Eq.(10) with

$$P_{k,l} = \frac{N_{\text{HOM}}^2 \binom{N}{k}^2 \binom{N}{l}^2}{2^{2N}} \left| (-1)^k + e^{i\phi_{\text{HOM}}} (-1)^l \right|^2 \times (B2)$$

$$(N-k)!k!(N-l)!l!$$

Simplifying with  $\binom{N}{k}^2 (N-k)!k! = N! \binom{N}{k}$  (and similarly for  $l$ ), we obtain the probabilities in Eq. (11) For  $k+l$  even we have  $(-1)^{k+l} = +1$ , so every term carries  $1 + \cos \phi_{\text{HOM}}$ :

$$P_{\oplus e} = \sum_{\substack{k,l=0 \\ k+l \text{ even}}}^N P_{k,l} = \frac{1 + \cos \phi_{\text{HOM}}}{2^{2N}} \sum_{\substack{k,l=0 \\ k+l \text{ even}}}^N \binom{N}{k} \binom{N}{l}. \quad (B3)$$

Using the binomial identities  $\sum_{k=0}^N \binom{N}{k} = 2^N$  and  $\sum_{k=0}^N (-1)^k \binom{N}{k} = 0$ , we obtain

$$\sum_{\substack{k,l=0 \\ k+l \text{ even}}}^N \binom{N}{k} \binom{N}{l} = \frac{1}{2} \sum_{k,l=0}^N [1 + (-1)^{k+l}] \binom{N}{k} \binom{N}{l}$$

$$= \frac{1}{2} \left( \sum_{k=0}^N \binom{N}{k} \right)^2 + \frac{1}{2} \left( \sum_{k=0}^N (-1)^k \binom{N}{k} \right)^2$$

$$= 2^{2N-1}, \quad (B4)$$

we get

$$P_{\oplus e} = \frac{1 + \cos \phi_{\text{HOM}}}{2} \quad (B5)$$

and similarly,

$$P_{\oplus o} = \frac{1 - \cos \phi_{\text{HOM}}}{2} \quad (B6)$$

which completes the derivation of Eq. (12).

---

[1] R. Colella, A. W. Overhauser, and S. A. Werner, Phys. Rev. Lett. **34**, 1472 (1975).

[2] M. Zych, F. Costa, I. Pikovski, and Č. Brukner, Nature Communications **2**, 505 (2011).

[3] H. Yu, D. Macri, T. Morling, E. Polini, T. B. Mieling, P. Barrow, B. Kabagöz, X. Yin, P. T. Chruściel, C. Hilweg, E. Oelker, N. Mavalvala, and P. Walther, arXiv:2511.17022 (2025).

[4] C. Overstreet, P. Asenbaum, J. Curti, M. Kim, and M. A. Kasevich, Science **375**, 226 (2022).

[5] I. Pikovski, M. Zych, F. Costa, and Č. Brukner, Nature Physics **11**, 668 (2015).

[6] S. Loriani, A. Friedrich, C. Ufrecht, F. D. Pumpo, S. Kleinert, S. Abend, N. Gaaloul, C. Meiners, C. Schubert, D. Tell, Étienne Wodey, M. Zych, W. Ertmer, A. Roura, D. Schlippert, W. P. Schleich, E. M. Rasel, and E. Giese, Science Advances **5**, eaax8966 (2019).

[7] A. Roura, Phys. Rev. X **10**, 021014 (2020).

[8] A. Roura, C. Schubert, D. Schlippert, and E. M. Rasel, Phys. Rev. D **104**, 084001 (2021).

[9] P. A. Bushev, J. H. Cole, D. Sholokhov, N. Kukharchyk, and M. Zych, New Journal of Physics **18**, 093050 (2016).

[10] M. Zych, F. Costa, I. Pikovski, T. C. Ralph, and Č. Brukner, Classical and Quantum Gravity **29**, 224010 (2012).

[11] J. Borregaard and I. Pikovski, Phys. Rev. Res. **7**, 023192 (2025).

[12] C. Fromonteil, D. V. Vasilyev, T. V. Zache, K. Hammerer, A. M. Rey, J. Ye, H. Pichler, and P. Zoller, arXiv:2509.19501 (2025).

[13] G. Sorci, J. Foo, D. Leibfried, C. Sanner, and I. Pikovski, arXiv:2509.09573 (2025).

[14] J. P. Covey, I. Pikovski, and J. Borregaard, PRX Quantum **6**, 030310 (2025).

[15] T. B. Mieling, C. Hilweg, and P. Walther, Phys. Rev. A **106**, L031701 (2022).

[16] R. Barzel, M. Gündoğan, M. Krutzik, D. Rätzel, and C. Lämmerzahl, Quantum **8**, 1273 (2024).

[17] P. K. Dahal and D. R. Terno, Phys. Rev. A **104**, 042610 (2021).

[18] J.-W. Pan, Z.-B. Chen, C.-Y. Lu, H. Weinfurter, A. Zeilinger, and M. Żukowski, Rev. Mod. Phys. **84**, 777 (2012).

[19] S. Clemmen, A. Farsi, S. Ramelow, and A. L. Gaeta, Phys. Rev. Lett. **117**, 223601 (2016).

[20] H.-H. Lu, M. Liscidini, A. L. Gaeta, A. M. Weiner, and J. M. Lukens, Optica **10**, 1655 (2023).

[21] D. Rieländer, A. Lenhard, O. Jiménez Fariñas, A. Mátta, D. Cavalcanti, M. Mazzera, A. Acín, and H. d. Riedmann, Quantum Science and Technology **3**, 014007 (2017).

- [22] J. M. Lukens and P. Lougovski, *Optica* **4**, 8 (2017).
- [23] H.-H. Lu, E. M. Simmernan, P. Lougovski, A. M. Weiner, and J. M. Lukens, *Phys. Rev. Lett.* **125**, 120503 (2020).
- [24] These states form decoherence-free subspaces, and therefore, constitute robust entanglement resources for long-distance and satellite-based entanglement assisted quantum networks.
- [25] X.-J. Wang, S.-J. Yang, P.-F. Sun, B. Jing, J. Li, M.-T. Zhou, X.-H. Bao, and J.-W. Pan, *Phys. Rev. Lett.* **126**, 090501 (2021).
- [26] K. S. Choi, *Coherent control of entanglement with atomic ensembles*, Phd thesis, California Institute of Technology (2011).
- [27] C. C. Gerry and J. Mimih, *Contemporary Physics* **51**, 497 (2010).
- [28] Éloi Descamps, A. Keller, and P. Milman, arXiv:2508.09887 (2025).
- [29] P. M. Anisimov, G. M. Raterman, A. Chiruvelli, W. N. Plick, S. D. Huver, H. Lee, and J. P. Dowling, *Phys. Rev. Lett.* **104**, 103602 (2010).
- [30] D. Lee, W. Shin, S. Park, J. Kim, and H. Shin, *Light: Science & Applications* **13**, 90 (2024).
- [31] J. P. Dowling, *Contemporary Physics* **49**, 125 (2008).
- [32] Y. Yang, *Opt. Express* **33**, 46426 (2025).
- [33] M. Gündoğan, P. M. Ledingham, K. Kothluer, M. Mazzera, and H. de Riedmatten, *Phys. Rev. Lett.* **114**, 230501 (2015).
- [34] Y. Ma, Y.-Z. Ma, Z.-Q. Zhou, C.-F. Li, and G.-C. Guo, *Nat. Commun.* **12**, 2381 (2021).
- [35] Y. O. Dudin, L. Li, and A. Kuzmich, *Phys. Rev. A* **87**, 031801 (2013).
- [36] E. Da Ros, S. Kanthak, E. Sağlamyürek, M. Gündoğan, and M. Krutzik, *Phys. Rev. Res.* **5**, 033003 (2023).
- [37] O. Katz and O. Firstenberg, *Nature Communications* **9**, 2074 (2018).
- [38] L. Esguerra, L. Meßner, E. Robertson, N. V. Ewald, M. Gündoğan, and J. Wolters, *Phys. Rev. A* **107**, 042607 (2023).
- [39] M. Jutisz, A. Erl, J. Wolters, M. Gündoğan, and M. Krutzik, *Phys. Rev. Appl.* **23**, 024045 (2025).
- [40] D. Lago-Rivera, S. Grandi, J. V. Rakonjac, A. Seri, and H. de Riedmatten, *Nature* **594**, 37 (2021).
- [41] X.-Y. Luo, Y. Yu, J.-L. Liu, M.-Y. Zheng, C.-Y. Wang, B. Wang, J. Li, X. Jiang, X.-P. Xie, Q. Zhang, X.-H. Bao, and J.-W. Pan, *Phys. Rev. Lett.* **129**, 050503 (2022).
- [42] V. Krutyanskiy, M. Galli, V. Krcmarsky, S. Baier, D. A. Fioretto, Y. Pu, A. Mazloom, P. Sekatski, M. Canteri, M. Teller, J. Schupp, J. Bate, M. Meraner, N. Sangouard, B. P. Lanyon, and T. E. Northup, *Phys. Rev. Lett.* **130**, 050803 (2023).
- [43] S. Merkouche, V. Thiel, A. O. C. Davis, and B. J. Smith, *Phys. Rev. Lett.* **128**, 063602 (2022).
- [44] I. Forbes, F. Ghafari, E. C. R. Deacon, S. P. Singh, E. Lavie, P. Yard, R. D. Shaw, A. Laing, and N. Tischler, arXiv:2502.00982 (2025).